Electronic Supplementary Information

Multifunctional Hierarchical 3-D ZnO Superstructures directly grown over FTO glass substrate: Enhanced Photovoltaic and Selective Sensing Applications

Mohammad Shaad Ansari[a], Avishek Banik[a], Anamika Kalita[b], Parameswar Krishnan Iyer [b,c] and Mohammad Qureshi[a*]

[a]Department of Chemistry, Indian Institute Technology Guwahati, Guwahati, 781039, India

[b]Centre for Nanotechnology, Indian Institute of Technology Guwahati, Guwahati, 781039, India

[c] Department of Chemistry, Indian Institute of Technology Guwahati, Guwahati, 781039, India.

Table of Contents

I. **Chemical Structure of Bio-mass derived templating agent ……S3**

II. **Probable Growth mechanism for in-situ grown hierarchical ZnO superstructures ……S3**

III. **Cross sectional FESEM images of in-situ grown hierarchical ZnO superstructures ……S5**

IV. **FESEM images of ZnO seed layer and complete morphological analysis of in-situ grown 1-D ZnO NWs, fabricated in absence of templating agent……S6**

V. **Digital Images related gas sensing experiment……S7**

VI. **Current-voltage (I-V) of both sensor devices……S8**

VII. **Gas sensing calibration plots for both sensor devices before measurements……S8**

VIII. **Steady state measurement for both sensor devices as a function of different concentration of NH_3 vapors ……S9**

IX. **Response of both sensor devices as a function of different concentration of NH_3 vapors……S10**

X. **Schematic representation of about probable sensing mechanism of NH_3 Vapors sensing……S10**

XI. **A comparative study of the in-situ grown ZnO heterostructures, sensitized with N719 dye based photovoltaic devices with different reported ZnO structures……S11**

I. Chemical Structure of Bio-template

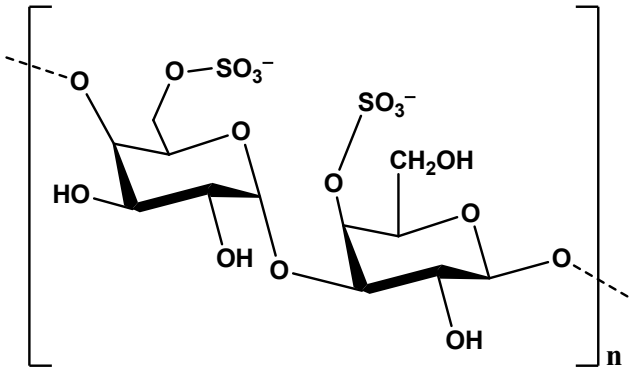

Figure S1. Chemical structure of bio-mass derived templating agent; "k-carrageenan".

II. Growth mechanism for the fabrication of ZnO superstructures

In accordance to morphological analysis, the plausible growth mechanism for the *in-situ* deposition of hierarchical 3-D ZnO superstructures over FTO substrate, under controlled hydrothermal reaction conditions is presented in figure S2. In general, growth process of the hierarchical 3-D superstructures can be triggered via two processes i.e., generation of primary structures and the crystal growth by means of secondary nucleation. It is anticipated that hierarchical 3-D superstructures are fabricated via assembling of primary ZnO structures i.e., 1-D ZnO NWs. Herein, water soluble and sulfate group containing an anionic polysaccharide "**k-carrageenan**" is utilized for monitoring the hetero epitaxial aggregated growth of 1-D nanocrystal. Natural hydrocolloid carrageenan is derived from red edible seaweed, having the repeating units of galactose and 3,6 anhydrogalactose (3,6-AG) and these repeating units are joined by alternating α-1,3 and β-1,4 glycosidic linkages, as shown in figure S1.

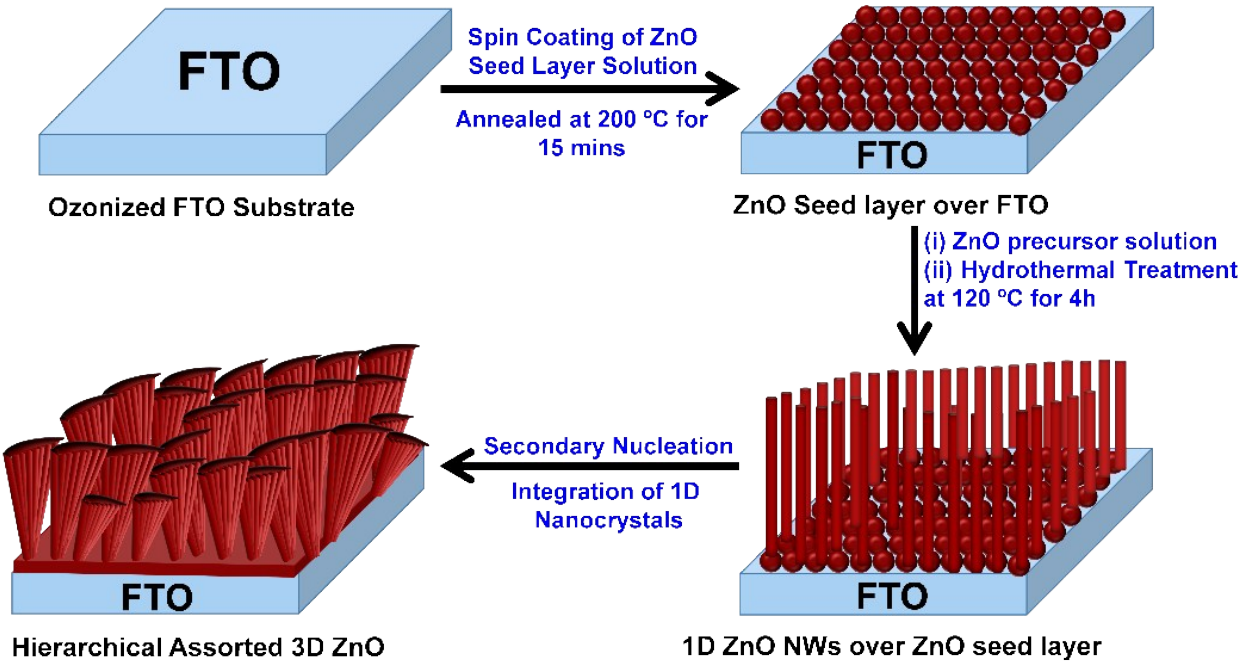

Figure S2. Schematic illustration of bio-mass derived template "k-Carrageenan" assisted in-situ growth of hierarchical 3D ZnO structures.

For direct deposition of hierarchical superstructures over conductive substrate, multinuclear ZnO seed layer was firstly deposited over precleaned ozonized FTO. This seed layer provided the specific growth sites for the epitaxial growth of 1-D ZnO nanocrystals. ZnO seeded FTO substrate (down side) was then immersed into the ZnO precursor solution and kept for hydrothermal reaction at 125 ^{o}C for 4 h for the growth of ZnO structures. ZnO precursor solution was prepared by dissolving the bio-template (1mg/mL) in the Milli-Q water which produced negative charged ions in solution because of hydroxyls and sulfate groups. After that, zinc nitrate was added into the reaction mixture and generated the positively charged Zn^{2+} ions in the solution. Thus, there is an electrostatic interaction between the negatively charged (OH^{-}/SO_3^{-}) and positively charged (Zn^{2+}) ions and generated adduct into the reaction mixture. Liquid ammonia ($NH_3 \cdot H_2O$) is then added into the reaction mixture which instantly produced a white precipitate of $Zn(OH)_2$. On continual addition of $NH_3 \cdot H_2O$, white precipitate turned into

clear solution, associated to the formation of $Zn(OH)_4^{2-}$ and $Zn(NH_3)_4^{2+}$ ions which acted as the crystal growth units for the formation of 1-D nanocrystals. Due to anisotropic nature of ZnO, growth units of ZnO favoured the crystal growth along the c-axis by minimizing the surface energy and encouraged the formation of epitaxial ZnO nanowires (NWs). In this growth mechanism, negatively charged k-carrageenan was utilized for the suppressing the crystal growth of ZnO NWs along the c-axis, resulting in the generation of non-uniform nanocrystals. During the secondary nucleation process, negatively charged biotemplate initiated the assembling of 1-D nanocrystals into a 3-D array to form hierarchical ZnO superstructures. After the complete nucleation of crystals, FTO substrate was expected to fully cover with the hierarchical 3-D ZnO superstructures. Therefore, we concluded that the highly oriented assembling of 1-D nanocrystals was controlled by the surface functionalities i.e., hydroxyl and sulfate groups present in the k-carrageenan. Moreover, generation of this kind of hierarchical structures is mainly attributed to anisotropic behaviour of ZnO crystal and dipole-dipole induced assembling of nanocrystals.

III. Cross sectional FESEM images of in-situ grown hierarchical ZnO structures

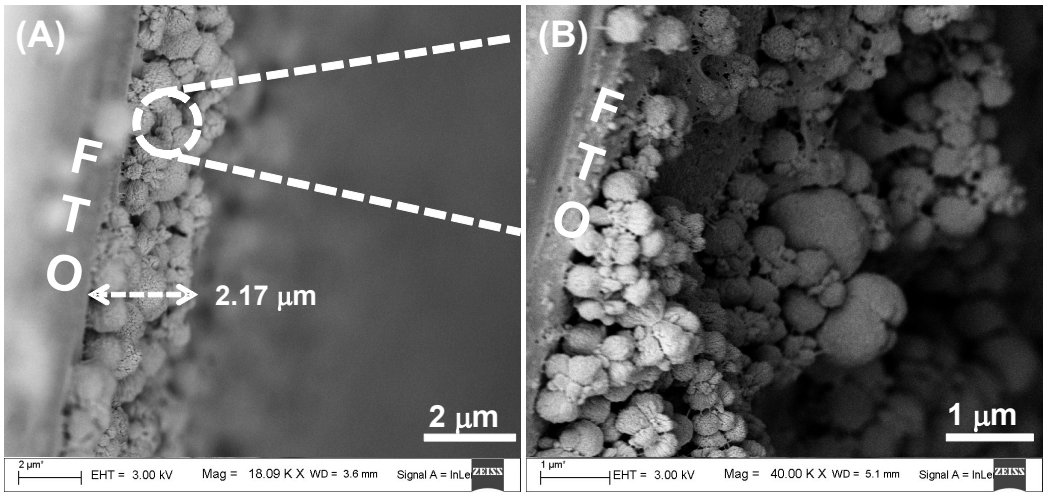

Figure S3. Images (A) and (B) show cross sectional view of in-situ deposited hierarchical 3D ZnO structures over FTO Glass Substrate.

IV. FESEM images of ZnO seed layer and complete morphological analysis of in-situ grown 1-D ZnO NWs, fabricated in absence of templating agent

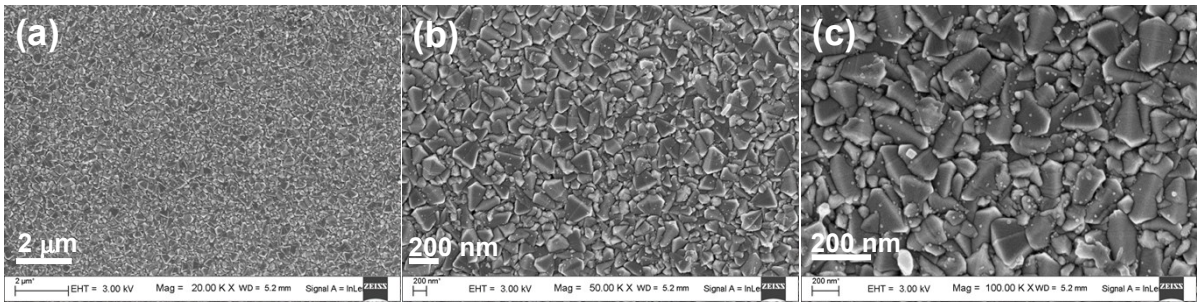

Figure S4. Images (a), (b) and (c) show top view of as-deposited seed layer of ZnO over FTO Glass Substrate.

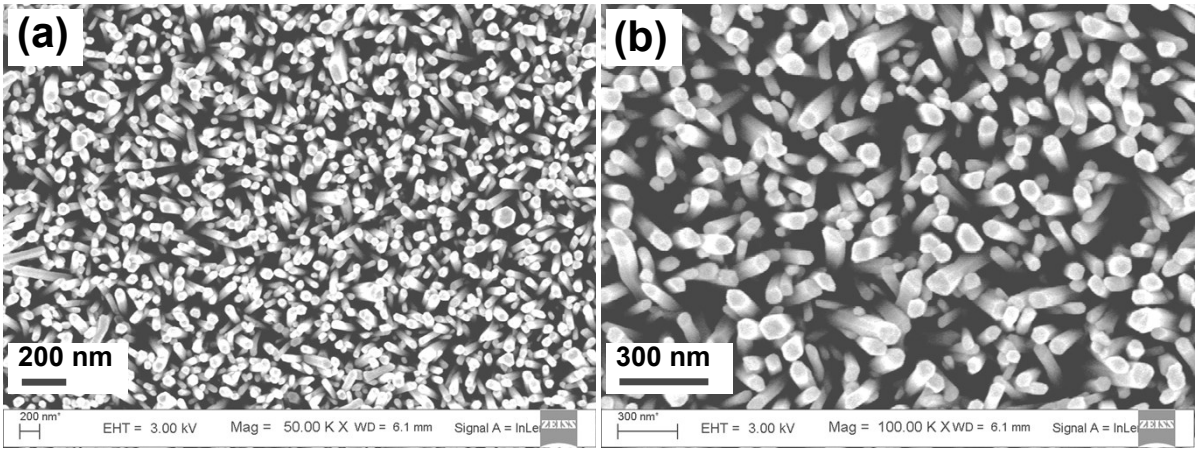

Figure S5. Images (a) and (b) show top view of as-deposited 1D ZnO NWs over FTO Glass Substrate.

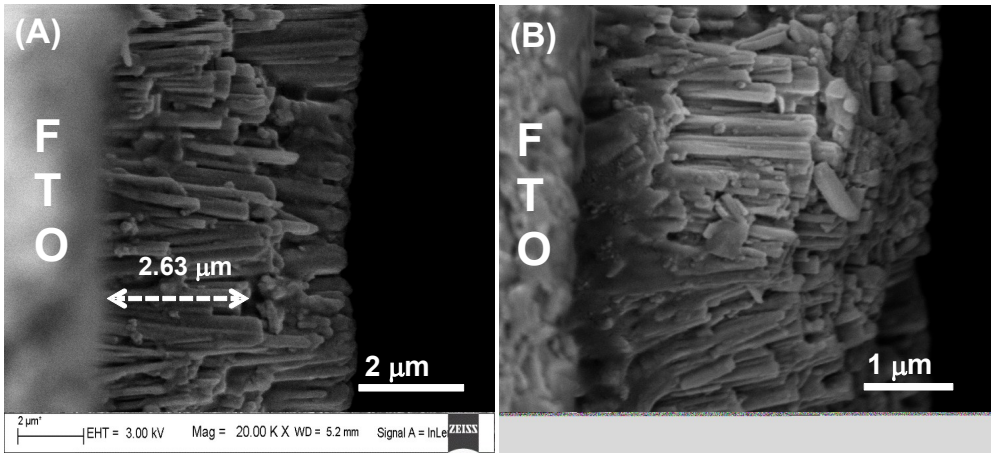

Figure S6. Images (a) and (b) show cross sectional view of as-deposited 1D ZnO NWs over FTO Glass Substrate.

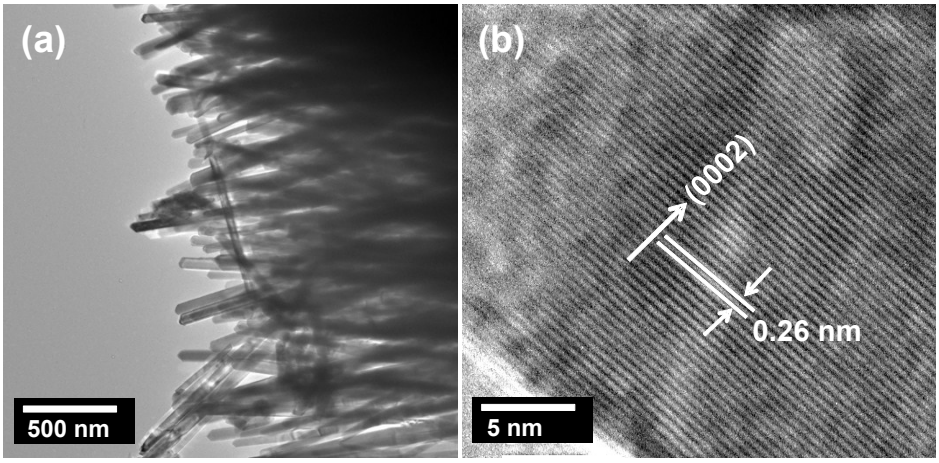

Figure S7. TEM image (a) shows the morphological features of in-situ grown 1-D ZnO NWs whereas high resolution TEM image (b) depicts the epitaxial growth 1D ZnO nanocrystals along the (0002) crystal plane.

VI. Digital Images of gas sensing assembly

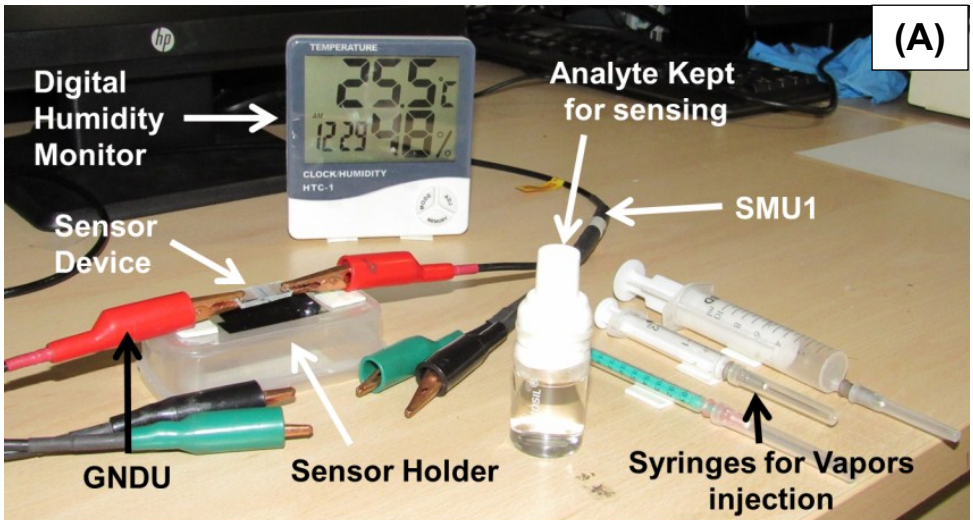

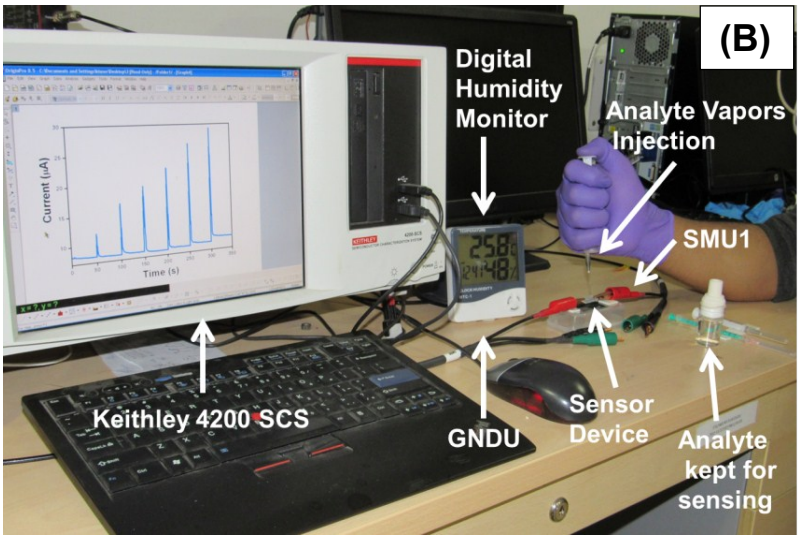

Figure S8. Digital Images (A & B) related to as-fabricated sensor device and experimental set-up for NH_3 gas sensing assembly.

VIII. Current-voltage (I-V) of both sensor devices

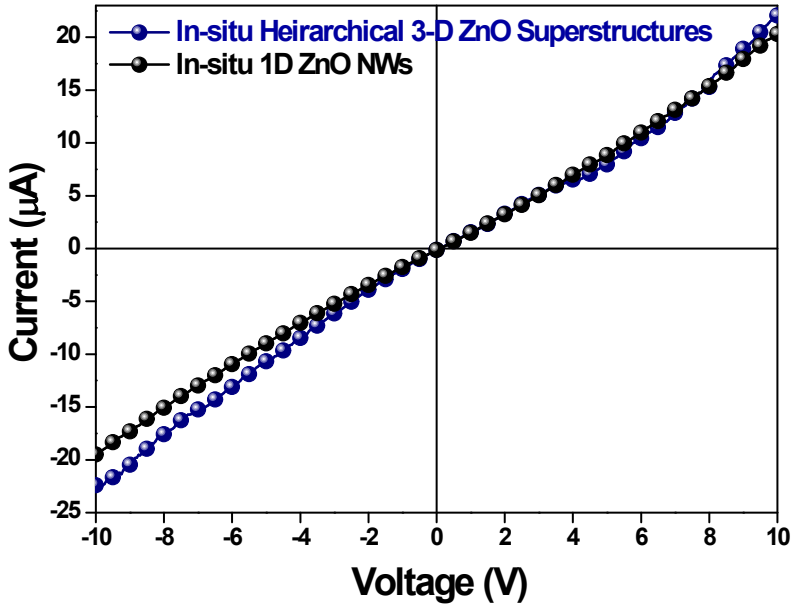

Figure S9. I–V curve for as-fabricated vapor phase sensing devices based on in-situ grown ZnO structures, recorded at room temperature with relative humidity of RH 53%.

IX. Gas sensing calibration plots for both sensor devices before measurements

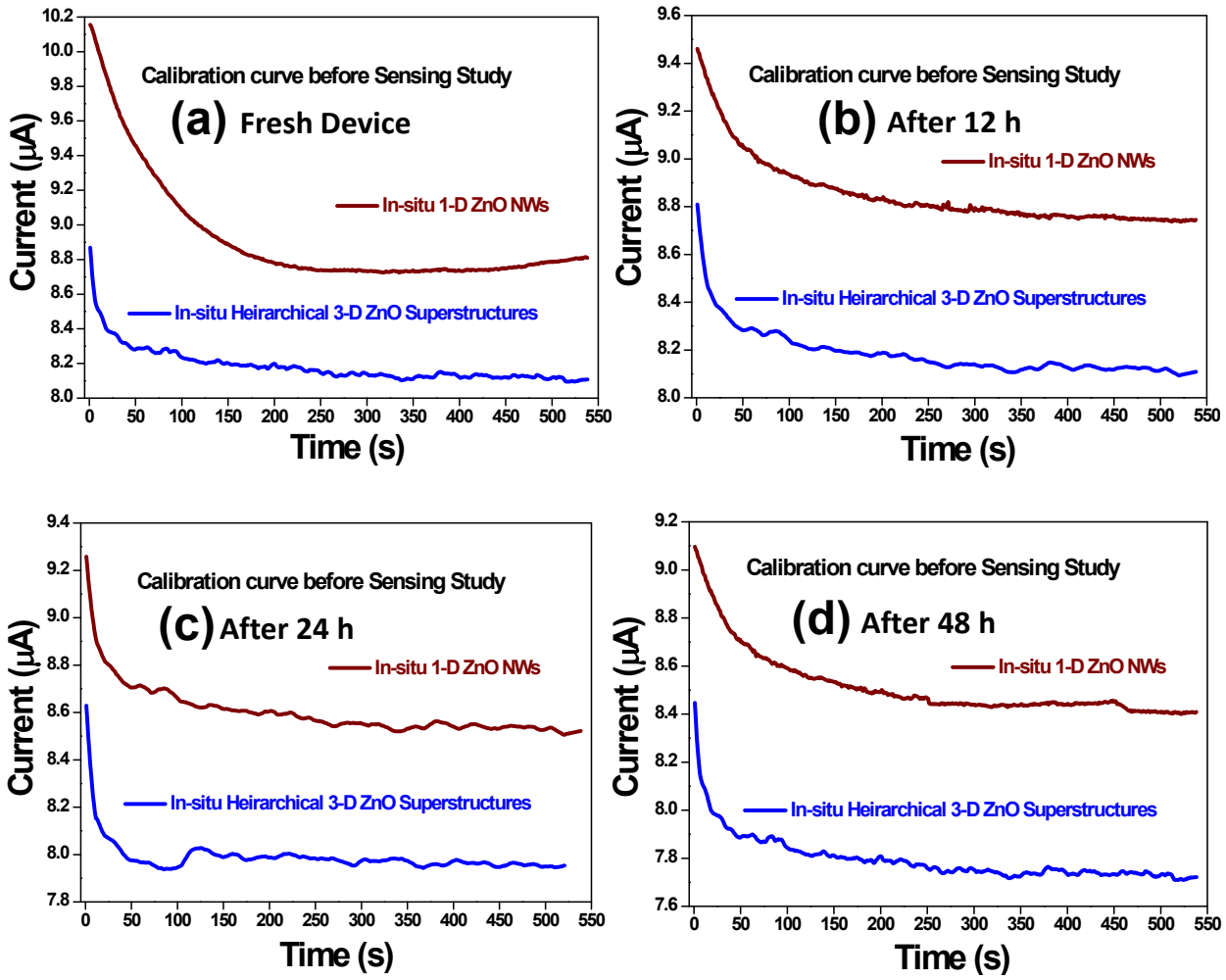

Figure S10. Gas sensing calibration curves for both in-situ grown heterostructures based sensor devices, measuring the current response as a function of time without injection of any analyte vapors with a regular interval upto few days under ambient condition at relative humidity of RH 52%.

X. Steady state measurement for both sensor devices as a function of different concentration of NH_3 vapors

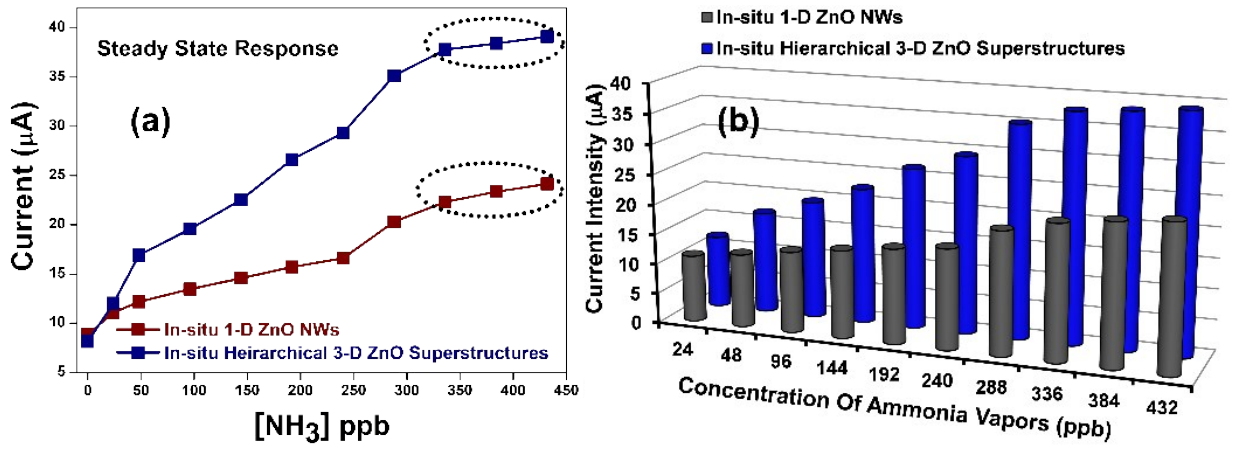

Figure S11. Plots (a) and (b) show the steady state current response for both vapor phase sensing devices based on in-situ grown ZnO structures with the different concentrations of NH_3 vapors, measured at room temperature with relative humidity level of RH 48%.

XI. Response of both sensor devices as a function of different concentration of NH_3 vapors

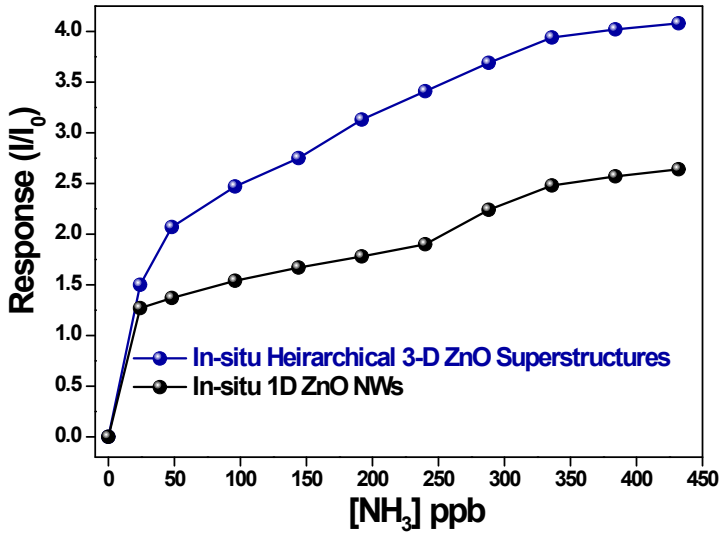

Figure S12. Response of both vapor phase sensing devices as a function of NH_3 concentration, performed at room temperature with relative humidity range of about RH 48%.

XII. Schematic representation of about probable sensing mechanism of NH_3 Vapors sensing

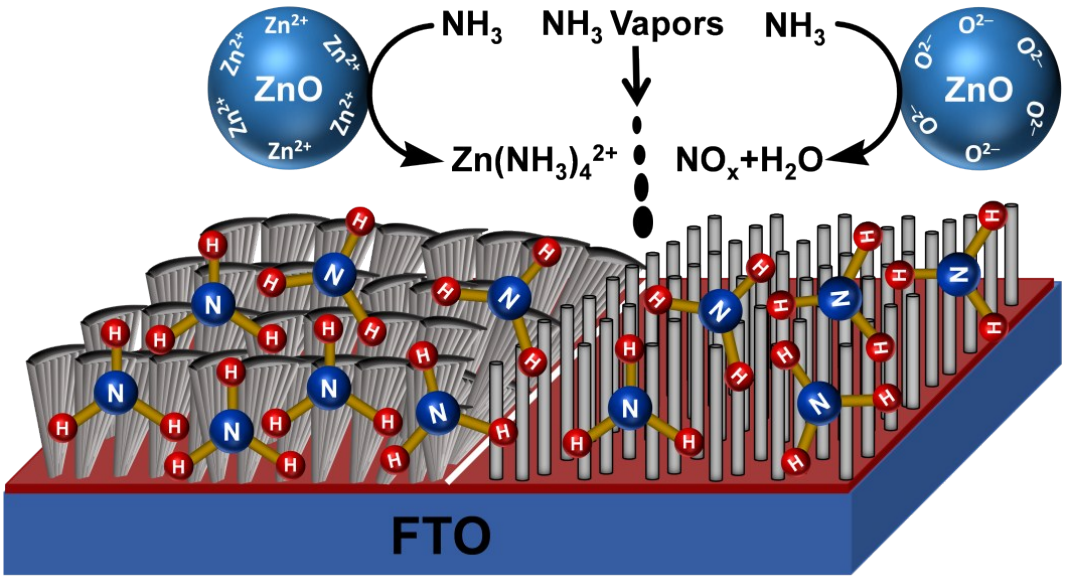

Figure S13. Schematic illustration represents the probable sensing mechanism.

Table S1. A comparative study of the in-situ grown ZnO heterostructures, sensitized with N719 dye based photovoltaic devices with different reported ZnO structures;

Reported ZnO Structures	Reagents	Sensitizer used	η (%)	Reference
ZnO porous nanosheets	Urea	N719	3.7	1
ZnO Nano flowers	NH_3	N719	1.9	2
ZnO Nanosheets	Urea: H_2O	N719	3.9	3
Branched ZnO Nanowires	Hexamethylenetetramine (HMTA) Polyethylenimine (PEI)	N719	1.51	4
ZnO nanoflowers	NH_3	N719	5.11	5
ZnO Nanoforest	HMTA, PEI	N719	2.63	6

Cactus ZnO	HMTA, NH_3	N719	3.09	7
ZnO Caterpillar-like	HMTA	N719	5.20	8
Hierarchical ZnO architectures	HMTA, trisodium citrate	N719	1.13	9
Cauliflower-like ZnO	Urea	N719	2.18	10
Nanospikes decorated ZnO sheets	Polyethylene glycol (PEG)	N719	2.51	11
ZnO Nanowire Array	HMTA, NH_3	N719	1.7	12
ZnO Nanowire Array	HMTA, PEI	N719	2.1	13
ZnO Nanofibers	Not mentioned (Sputtering)	Indoline dye	1.66	14
ZnO Nanoribbon	HMTA, NaOH	N719	2.41	15
Hierarchical ZnO Nanorod/Nanosheet	Not mentioned (Electrodeposition)	N719	3.12	16
Hierarchical ZnO nanowire-nanosheet	Not mentioned (Electrodeposition)	N719	4.80	17
ZnO Nanoflakes	NaOH	N719	4.50	18
ZnO nanorod/nanoparticle hierarchical structure	KOH	N719	3.63	19
1-D ZnO Nanowires	NH_3	N719	2.57	Present Manuscript
Hierarchical 3-D ZnO Superstructures	**k-carrageenan, Dil. NH_3**	**N719**	**3.83**	**Present Manuscript**

References

1. X. Y. Wang, Z. P. Tian, T. Yu, H. M. Tian, J. Y. Zhang, S. K. Yuan, X. B. Zhang, Z. S. Li and Z. G. Zou, *Nanotechnology*, 2010, **21**, 1–5.
2. C. Y. Jiang, X. W. Sun, G. Q. Lo, D. L. Kwong and J. X. Wang, *Appl. Phys. Lett.*, 2007, **90,** 1–3.
3. E. Hosono, S. Fujihara, I. Honna and H. S. Zhou, *Adv. Mater.*, 2005, **17**, 2091–2094.
4. H. M. Cheng, W. H. Chiu, C. H. Lee, S. Y. Tsai and W. F. Hsieh, *J. Phys. Chem. C*, 2008, **112**, 16359–16364.
5. B. Kilic, T. Gunes, I. Besirli, M. Sezginer and S. Tuzemen, *Appl. Surf. Sci.*, 2014, **318**, 32–36.
6. S. H. Ko, D. Lee, H. W. Kang, K. H. Nam, J. Y. Yeo, S. J. Hong, C. P. Grigoropoulos and H. J. Sung, *Nano Lett.*, 2011, **11**, 666–671.
7. P. Baviskar, R. Gore, A. Ennaoui and B. Sankapal, *Mater. Lett.*, 2014, **116**, 91–93
8. M. McCune, W. Zhang and Y. L. Deng, *Nano Lett*, 2012, **12**, 3656–3662.
9. S. B. Zhu, L. M. Shan, X. N. Chen, L. He, J. J. Chen, M. Jiang, X. L. Xie and Z. W. Zhou, *RSC Adv.*, 2013, **3**, 2910–2916.
10. Y. Q. Wang, X. Cui, Y. Zhang, X. R. Gao and Y. M. Sun, *J. Mater. Sci. Technol.*, 2013, **29**, 123–127.
11. S. Ameen, M. S. Akhtar and H. S. Shin, *Chem. Eng. J.*, 2012, **195**, 307–313.
12. Y. F. Gao, M. Nagai, T. C. Chang and J. J. Shyue, *Cryst. Growth Des.*, 2007, **7**, 2467–2471.
13. C. K. Xu, P. Shin, L. L. Cao and D. Gao, *J. Phys. Chem. C*, 2010, **114**, 125–129.
14. O. Lupan, V. M. Guérin, L. Ghimpu, I. M. Tiginyanu and T. Pauporté, *Chem. Phys. Lett.*, 2012, **550**, 125–129.
15. Z. Li, D. Bi, Y. Zhao, R. Liu, J. Ye and Y. Zhou, *Electrochim. Acta*, 2018, **262**, 124–134.

16. J. Qiu, M. Guo and X. Wang, *ACS Appl. Mater. Interfaces*, 2011, **3**, 2358–2367.

17. F. Xu, M. Dai, Y. Lu and L. Sun, *J. Phys. Chem. C*, 2010, **114**, 2776–2782.

18. C. Zhao, J. Zhang, Y. Hu, N. Robertson, P. A. Hu, D. Child, D. Gibson and Y. Q. Fu, *Sci. Rep.*, 2015, **5**, 17750.

19. R. Gao, Y. Cui, X. Liu, L. Wang and G. Cao, *J. Mater. Chem. A*, 2014, **2**, 4765–4770.